

Fusion of Evidences for Edge Detection in PolSAR Images

Anderson Adaime de Borba - Mackenzie-BR - IBMEC-SP

Dr. Mauricio Marengoni - Mackenzie-BR

Dr. Alejandro Frery - UFAL-BR

October 30, 2019

IBMEC-SP - 2019

PolSAR important characteristics

- can be on raised platforms, crewed aircraft or not, satellites orbiting the earth or other planets;
- it is a viable and practical imaging technique;
- PolSAR images has a high resolution;
- synthesizes long antenna openings;
- radars produce images day and night;
- climate does not interfere in image capture.
- SAR imaging systems operate in the microwave region of the electromagnetic spectrum, usually between the P-band - and the K-band.

Economy Applications

- EOxposure- Project with European Union ;
- The goal of the EOxposure project is to build tools to quantify the exposure of population and economic assets to multiple risks using novel information layers from current and future Earth Observation (EO) missions, as well as the growing sensor web on the ground;
- Housing condition mapping;
- Disease spread proxies;
- Physical proxies to security threats.

Economy Applications - The Gross Domestic Product - GDP

- Article address;
- We estimate a TVP VAR via maximum likelihood;
- The stochastic volatility of the system is modeled via a Wishart process.
- The law of motion of VAR coefficients allows for multivariate stochastic volatility;
- The likelihood function of this model and all filtering formulas for tracking the latent states are obtained in closed form.

Economy Applications - The View from Above: Applications of Satellite Data in Economics

- Article address;
- Forest Cover over Time in Riau Province, Indonesia;
- Aerosol Index of Particulate Air Pollution in Indonesia during Massive Wildfires in 1997;
- Roofs in Kibera, Nairobi;

PolSAR Image

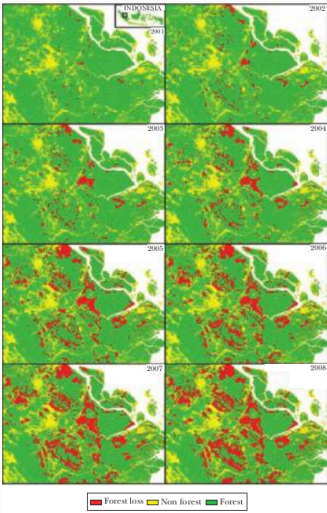


Figure 1: Forest Cover over Time in Riau Province, Ref. [1]

PolSAR Image

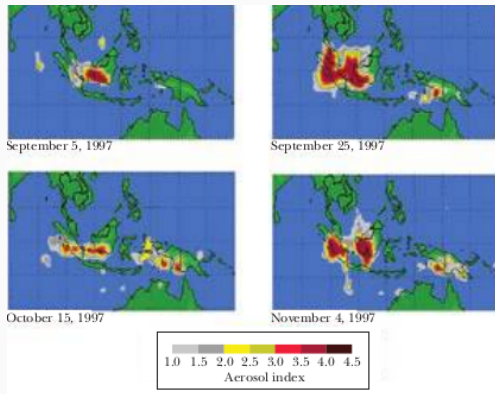


Figure 2: Aerosol Index of Particulate Air Pollution in Indonesia, Ref. [1]

PolSAR Image

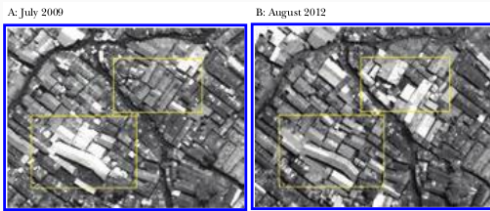


Figure 3: Roofs in Kibera, Nairobi, Ref. [1]

Statistical modeling for PolSAR data (1 - Look)

- The complex scattering matrix \mathbf{S} :

$$\mathbf{S} = \begin{bmatrix} S_{hh} & S_{hv} \\ S_{vv} & S_{vv} \end{bmatrix}. \quad (1)$$

- The medium of propagation of waves is reciprocal

$$\mathbf{s} = [S_{hh}, S_{hv}, S_{vv}]^T.$$

Statistical modeling for PolSAR data (1 - Look)

- The probability density function (pdf):

$$f_s(s; \Sigma) = \frac{1}{\pi^3 |\Sigma|} \exp(-s^H \Sigma^{-1} s), \quad (2)$$

- $|\cdot|$ is the determinant,
- H denotes the conjugate complex number,
- Σ is the covariance matrix of s such that $\Sigma = E[ss^H]$,
- $E[\cdot]$ denotes the expected value.
- The distribution of s is assumed to be Gaussian circular complex multivariate with zero mean $N_3^C(0, \Sigma)$.

Statistical modeling for PolSAR data (L - Looks)

- The estimated sample covariance matrix:

$$\mathbf{Z} = \frac{1}{L} \sum_{\ell=1}^L \mathbf{s}_\ell \mathbf{s}_\ell^H, \quad (3)$$

- \mathbf{s}_ℓ , $\ell = 1, \dots, L$;
- L independent samples of complex vectors distributed as \mathbf{s} .

Statistical Modeling

Statistical modeling for PolSAR data (L - Looks)

- Multilooked Wishart distribution with probability density function:

$$f_{\mathbf{Z}}(\mathbf{Z}; \Sigma_s, L) = \frac{L^{mL} |\mathbf{Z}|^{L-m}}{|\Sigma_s|^L \Gamma_m(L)} \exp(-L \operatorname{tr}(\Sigma_s^{-1} \mathbf{Z})), \quad (4)$$

- $\operatorname{tr}(\cdot)$ is the trace operator,
- $\Gamma_m(L)$ is a multivariate Gamma function

$$\Gamma_m(L) = \pi^{\frac{1}{2}m(m-1)} \prod_{i=0}^{m-1} \Gamma(L-i),$$

- $\Gamma(\cdot)$ is the Gamma function,
- $m = 3$,
- $\mathbf{Z} \sim W(\Sigma, L)$,

Edges detection

Method

The following procedure is proposed to detected edges in the hh, hv and vv channels:

- identify the centroid of a region of interest (ROI) in an automatic, semi-automatic or manual manner;
- cast rays from the centroid to the outside of the area;
- collect data around the rays using the Bresenham's midpoint line algorithm, ideally the size of a pixel;
- detect points in the data strips which provide evidence of changes in their statistical properties, i.e., a transition point that defines edge evidence;
- use the Generalized Simulated Annealing (GenSA) method, Ref. [2], to find maximum points in the functions of interest;
- fuse the evidence of detected edges in the hh, hv and vv channels.

Edges detection

ROI Flevoland Example

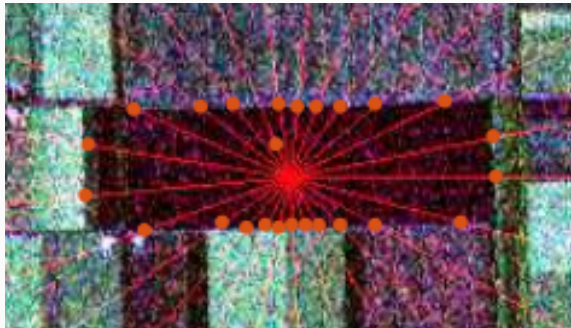


Figure 4: Edges detection example (hh channel).

Maximum Likelihood Estimator (MLE)

- Suppose $\mathbf{X} = (X_1, X_2, \dots, X_n)^T$ is a random vector distributed according to the probability density function $f(\mathbf{x}, \theta)$ with parameters $\theta = (\theta_1, \dots, \theta_d)^T$ in the parameter space Θ .
- The likelihood function is

$$L(\theta; \mathbf{X}) = \prod_{i=1}^n f(x_i; \theta),$$

- log-likelihood function is

$$\ell(\theta; \mathbf{X}) = \ln L(\theta; \mathbf{X}) = \sum_{i=1}^n \ln f(x_i; \theta), \quad (5)$$

- $\hat{\theta} = \arg \max_{\theta \in \Theta} L(\theta; \mathbf{x}),$
- $\hat{\theta} = \arg \max_{\theta \in \Theta} \ell(\theta; \mathbf{x}).$

Edges detection

Maximum Likelihood Estimator (MLE) for two regions A and B

- The estimates for the covariance matrices can be found using the maximum likelihood estimator denoted by $\widehat{\Sigma}$, Ref. [3]:

$$\widehat{\Sigma}_l(j) = \begin{cases} j^{-1} \sum_{k=1}^j \mathbf{Z}_k & \text{if } l = A, \\ (N-j)^{-1} \sum_{k=j+1}^N \mathbf{Z}_k & \text{if } l = B. \end{cases} \quad (6)$$

- likelihood function

$$L(j) = \prod_{k_1=1}^j f_{\mathbf{Z}}(\mathbf{Z}_{k_1}; \widehat{\Sigma}_A, L) \prod_{k_2=j+1}^N f_{\mathbf{Z}}(\mathbf{Z}_{k_2}; \widehat{\Sigma}_B, L), \quad (7)$$

- log-likelihood function

$$\ell(j) = \sum_{k_1=1}^j \ln f_{\mathbf{Z}}(\mathbf{Z}_{k_1}; \widehat{\Sigma}_A, L) + \sum_{k_2=j+1}^N \ln f_{\mathbf{Z}}(\mathbf{Z}_{k_2}; \widehat{\Sigma}_B, L). \quad (8)$$

Maximum Likelihood Estimator (MLE)

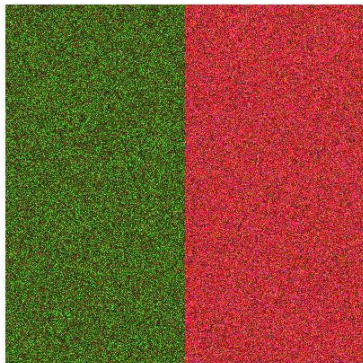
- After algebraic manipulations on each term of the summation, it is obtained:

$$\begin{aligned}\ell(j) = & N[mL(\ln L - 1) - \ln \Gamma_m(L)] \\ & - L \left[j \ln |\widehat{\Sigma}_A(j)| + (N-j) \ln |\widehat{\Sigma}_B(j)| \right] \\ & + (L-m) \sum_{k=1}^N \ln |\mathbf{Z}_k|. \end{aligned} \tag{9}$$

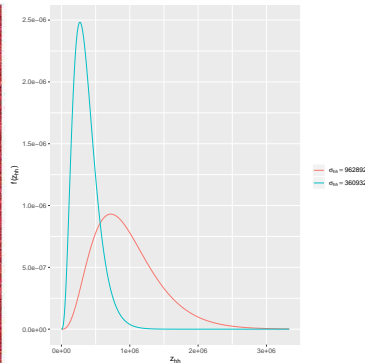
- The argument of the maximum \widehat{j} is the edge evidence that will be used in our fusion methods.

Edges detection

Application in simulated images



(a) Pauli decomposition



(b) Marginal densities of the hh channel

Figure 5: Model and observations

Edges detection

Application in simulated images

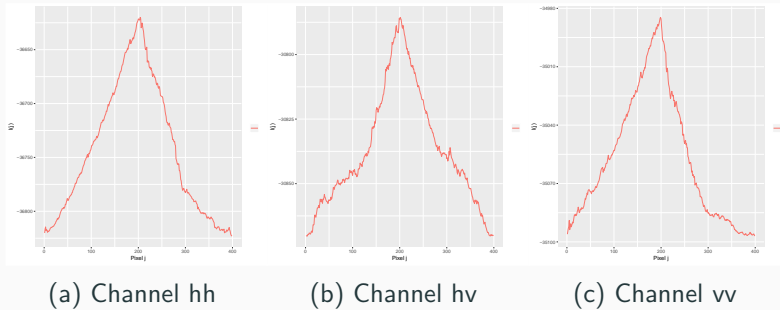


Figure 6: $I(j)$ log-likelihood function

Edges detection

Application in simulated images

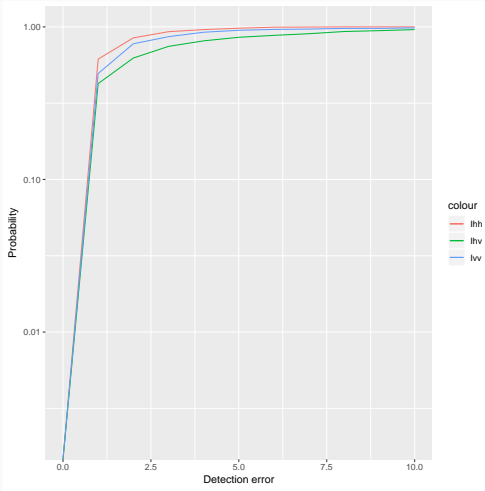


Figure 7: Probability of detecting edges evidences.

Evidence Fusion

Average Fusion

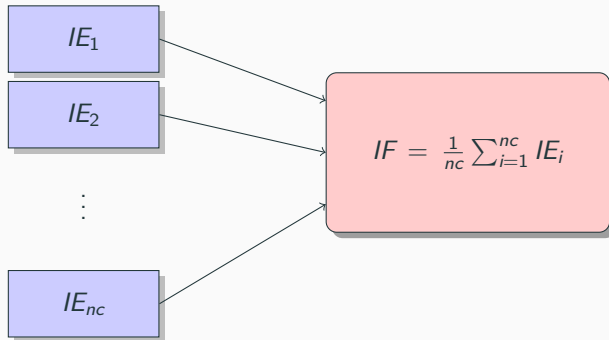


Figure 8: Average Fusion.

Evidence Fusion

PCA Fusion

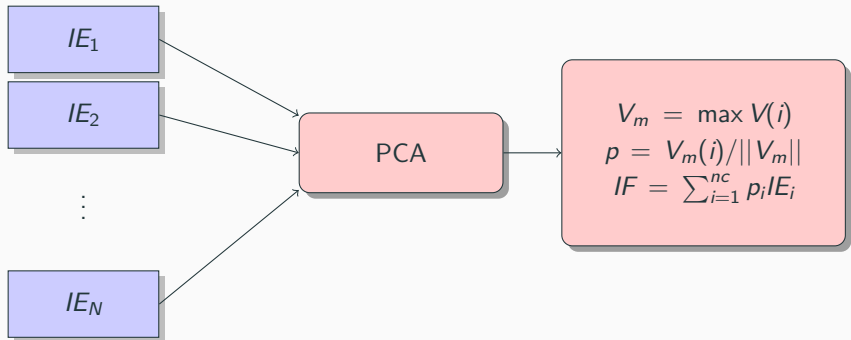


Figure 9: PCA Fusion.

Evidence Fusion

Stationary wavelet transform – SWT Fusion

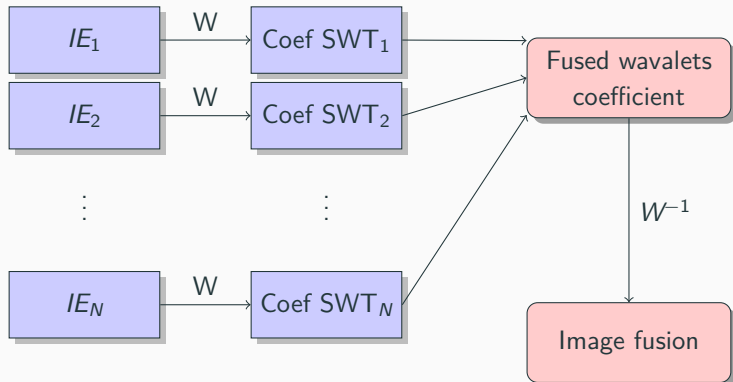


Figure 10: SWT Fusion.

- W is wavelet transformed.

Conclusion

Discrete wavelet transform – DWT Fusion

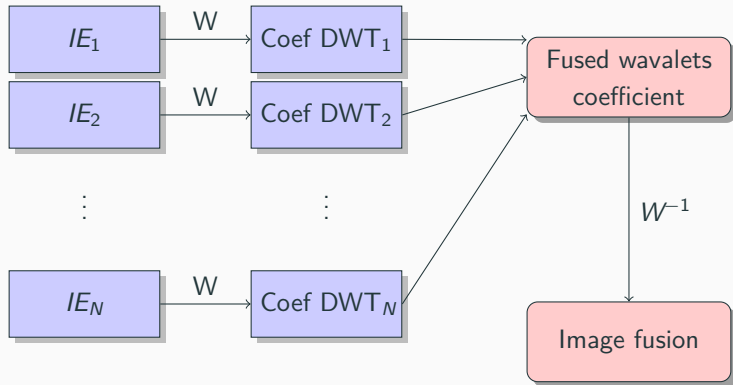


Figure 11: DWT Fusion.

Evidence Fusion

ROC statistics Fusion

- Part I

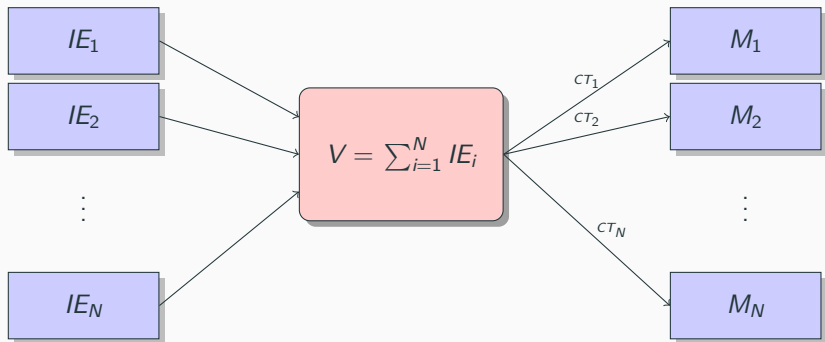


Figure 12: Fusion based in ROC statistics - Part I.

- CT_i is a threshold.

Evidence Fusion

ROC statistics Fusion

- Part II - for each M_j

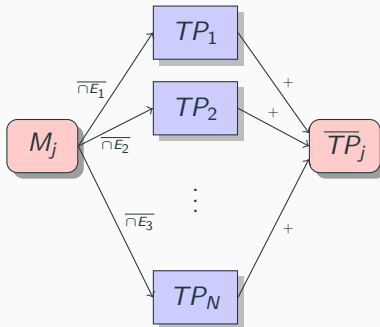


Figure 13: ROC Fusion for each j . It is true to \overline{TN}_j , \overline{FP}_j and, \overline{FN}_j .

- To generate the confusion matrix, and calculate the ROC statistics.

Results

Results

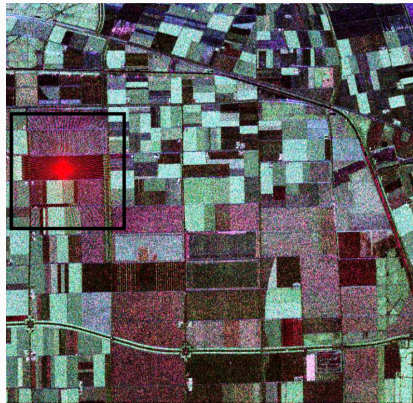


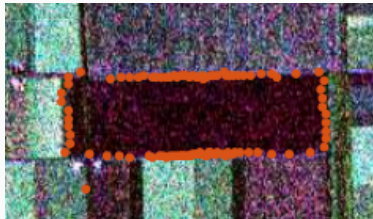
Figure 14: Region of interest (ROI) in the image of Flevoland.

Results

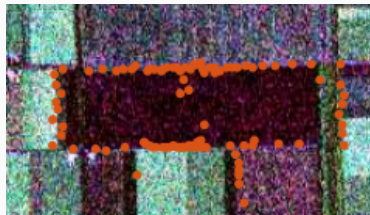
Results



(a) Evidences in channel hh



(b) Evidences in channel hv



(c) Evidences in channel vv

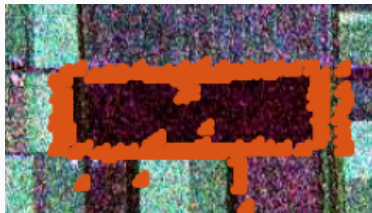
Results



(a) Average Fusion



(b) PCA Fusion



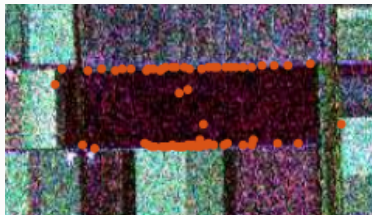
(c) DWT Fusion



(d) SWT Fusion

Figure 16: Evidence after fusion

Results



(a) ROC Fusion



(b) SVD Fusion

Figure 17: Evidence after fusion

Conclusion

Conclusion

- Simulated Annealing works very well in non differentiable function. Figure (7) shows the probability of detecting edges evidences;
- The method to detect edges evidence in each channel works very well. See Figure (15). Similar ideas can be found in Refs. [4, 5];
- The fusion of evidence in intensity channels shows that these channels can be complementary and, therefore, suitable for edge detection in PolSAR images. See Figure (17).
- The article shows the viability of these methods and your extension to more channels.

Future researches

- Increase the number of channels to improve the fusion;
- Investigate new fusion methods.

-  D. Donaldson and A. Storeygard, "The View from Above: Applications of Satellite Data in Economics," *Journal of Economic Perspectives*, vol. 30, no. 4, pp. 171–198, Fall 2016. [Online]. Available:
<https://ideas.repec.org/a/aea/jecper/v30y2016i4p171-98.html>
-  Yang Xiang, S. Gubian, B. Suomela, and J. Hoeng, "Generalized simulated annealing for efficient global optimization: the GenSA package for R." *The R Journal Volume 5/1, June 2013*, 2013. [Online]. Available:
<https://journal.r-project.org/archive/2013/RJ-2013-002/index.html>
-  N. R. Goodman, "The distribution of the determinant of a complex wishart distributed matrix," *Ann. Math. Statist.*, vol. 34, no. 1, pp. 178–180, 03 1963. [Online]. Available:
<http://dx.doi.org/10.1214/aoms/1177704251>

-  A. C. Frery, J. Jacobo-Berlles, J. Gambini, and M. Mejail, “Polarimetric SAR image segmentation with b-splines and a new statistical model,” *CoRR*, vol. abs/1207.3944, 2012.
-  A. Nascimento, M. Horta, A. Frery, and R. Cintra, “Comparing edge detection methods based on stochastic entropies and distances for polsar imagery,” *Journal of Selected Topics in Applied Earth Observations and Remote Sensing*, vol. 7, no. 2, pp. 648–663, 2014.